Solvent mode participation in the non-radiative relaxation of the hydrated electron

Oleg V. Prezhdo and Peter J. Rossky

Department of Chemistry and Biochemistry
University of Texas at Austin
Austin, Texas 78712-1167

Abstract

Non-adiabatic molecular dynamics simulations are used to analyze the role of different solvent degrees of freedom in the non-radiative relaxation of the first excited state of the hydrated electron. The relaxation occurs through a multi-mode coupling between the adiabatic electronic states. The process cannot be described by a single mode promotion model frequently used in the "large molecule" limit of gas phase theories. Solvent librations and vibrations, and the H_2O asymmetric stretch in particular, are found to be the most effective promotors of the electronic transition. Dissipation of the released energy to the solvent proceeds on two time scales: a fast 10-20 fs heating of the first solvation shell, where most of the energy is accepted by the librational degrees of freedom, and a several hundred femtosecond global reconstruction of the solvent as the first shell transfers its excess energy to the rest of the molecules. The implications of our use of a semiclassical approximation as the criterion for good promoting and accepting modes are discussed.

1

1 Introduction

The majority of chemical processes involve radiationless energy transfer in one or more of their elementary steps, be it an intermolecular conversion, intramolecular relaxation, or an ordinary heating necessary to activate a reaction. The role of non-radiative processes is particularly pronounced in liquid phase chemistry, where the solvent serves as a thermal bath providing or withdrawing energy from the reacting species. During the last decade new experimental and theoretical techniques have been developed allowing for detailed dynamical studies on ultrafast processes in polar solutions. The hydrated electron, being a relatively simple as well as ubiquitous species in solution photo- and electrochemistry, represents a unique system for such studies. Because the hydrated electron is merely an extra electron in pure water, its evolution is governed solely by nuclear motions of water molecules. The instantaneous configuration of the solvent determines the Born-Oppenheimer (B-O) electronic energy spectrum. Vibrations and librations couple these electronic states leading to non-adiabatic radiationless transitions. The electronic energy released during the transitions is accepted by specific solvent modes, and, as the solvation structure approaches equilibrium, the energy is dissipated into the rest of the solvent. The present work was carried out to elucidate in detail what particular solvent motions and solvent regions have the greatest impact on these aspects of hydrated electron relaxation dynamics. This analysis represents the first such detailed examination for an electronic relaxation in solution.

The idea of non-radiative paths of energy transfer between states of two species was born in photon absorption and emission experiments. The first recorded evidence of radiationless processes dates back to 1923, when Cario and Frank[1] studied emission spectra of mercury–thallium gaseous mixtures irradiated by light resonant with an electronic transition of mercury atoms. Emission spectra showed both mercury and thallium lines suggesting that a fraction of mercury atoms non-radiatively transferred their excess energy to thallium atoms. Experimental studies on radiationless relaxation in isolated molecules were first carried out in the 1960's.[2,3] The results were interpreted using a molecular energy level scheme based on the

Born-Oppenheimer separability of electronic and nuclear degrees of freedom. Non-radiative relaxation of excited adiabatic electronic states was explained in terms of vibronic coupling treated perturbatively (Fermi Golden Rule).[4−7] The complexity of the problem lies in the huge dimensionality of vibronic basis sets, and often further approximations are involved, the most well-known being the introduction of Franck-Condon factors. Intramolecular radiationless processes within relatively small isolated molecules were extensively studied both experimentally and theoretically.[8−12] Several new concepts were introduced, such as promoting modes – those which induce non-radiative electronic transitions between B-O states, and accepting modes – those that accommodate the energy released during such transitions, when these occur at points away from curve crossings. Depending on the number of vibrations that couple electronic states, "large" and "small" molecule limits were suggested. Many theoretical techniques were used to treat vibronic Hamiltonians: Laplace transformation, Green's function, projection operator, effective Hamiltonian methods, and wave packet formalism.[8]

Molecular energy transfer in condensed media is a less developed subject[13,14] and is notably based on the gas phase theories. Experiments on luminescence of large molecules in solutions were conducted[15−17] prior to the corresponding experiments in gas phase.[2,3] However, they provided less detailed data. Theoretical description of the results of condensed phase measurements is complex due to the presence of a solvent which both accepts released energy and contributes to relaxation promotion. In the case of monoatomic solutes (including the hydrated electron) solvent motion alone is responsible for the coupling between adiabatic electronic states. In the simplest form the solvent can be described by its macroscopic characteristics (viscosity and dielectric response) leading to continuum models. Although such models still play a major role in some areas[18−20], they cannot reproduce ultrafast solvent dynamics on the time scale of motions of individual molecules. Molecular dynamics methods consider solute-solvent systems in their full molecularity and thus are more suitable for simulations of energy transfer processes in solutions. A short time approximation to the evolution

of molecular trajectories leads to another ansatz – instantaneous normal modes.[21,22] At each instance of time, the solvent is regarded as a single large molecule characterized by a quasi-continuous spectral density of vibrational states. The model of a harmonic bath coupled to a solute was successful in a generic description of vibrational relaxation in condensed media[13], and harmonic baths are also widely used in other areas, such as quantum decoherence[23,24], tunneling[25,26] and Brownian motion.[27]

Recent advances in time resolved spectroscopies[28−33], and parallel theoretical research[34−42] has made the aqueous solvated electron an exceptional probe of dynamics of chemical processes in polar solvents.[43−45] The hydrated electron is a relatively simple system from the theoretical point of view. It is also tractable by spectroscopic techniques due to its large optical cross-section. At the same time, the hydrated electron exhibits a remarkably rich dynamical picture: the hydrated electron excited electronic state relaxation is intimately intertwined with the configurational rearrangement of the solvent as evidenced by recent experimental studies[32,33] involving photoexcitation of the equilibrium ground state and subsequent nonradiative relaxation back to the ground state, as well as by earlier experiments[28−31] on hydrated electrons created by a multiphoton ionization of pure water at much higher energies. Many aspects of the electron evolution have been elucidated via theoretical analysis employing simulated dynamics and comparison to experiment.[46−53]

The present paper focuses on the previously unexplored aspect associated with the identification of particular modes of water molecules that most strongly couple adiabatic states of the hydrated electron (promoting modes), and those that provide effective sinks for the energy released during non-adiabatic radiationless transitions (accepting modes), and also during the subsequent adiabatic relaxation of the electron. The next section deals with the criteria for good promoting and accepting modes and the implications of our use of a semi-classical approach. We then discuss in Sec. 3 the excess-electron-in-water system in detail and, finally, summarize our conclusions in Sec. 4.

2 Theory

The results here are obtained from simulations based on a variant of non-adiabatic molecular dynamics devised by Webster *et al.*[37], which incorporates a semiclassical force on the solvent[54] derived via a path integral formulation[55] and employs a surface hopping technique [56,57] for determining transition rates. For our studies we use the results of earlier simulations.[48] The model consists of 200 classical SPC flexible water molecules[58,59] and an electron treated quantum mechanically. The electron–water pseudopotential was taken from earlier work.[60] Twenty non-adiabatic trajectories were considered, characterized by solvent density 0.997 g/cm^3 at room temperature. Each of the trajectories was initiated from a configuration of an adiabatically equilibrated electron in its ground state. The electron was then instantaneously promoted to the first excited state and allowed to non-adiabatically relax back to the ground state.

2.1 Separation of solvent contributions by modes and space

To draw physically clear conclusions about the role of the solvent in the electron relaxation, a convenient coordinate system for the solvent degrees of freedom is needed. We use the following scheme to separate the overall solvent motion into the subsets of internal motions of individual molecules. For each water molecule we define the translational degrees of freedom by separating the center of mass motion and the three rotational modes by diagonalizing the instantaneous moment of inertia tensor. To define the vibrational modes one could expand the potential acting on the molecule up to second order terms in the displacement from the instantaneous configuration. Diagonalization of the corresponding Hessian matrix would produce the normal modes and the vibrational frequencies. However, a water molecule in solution can be substantially distorted (in our simulations the H–O–H angle and O–H bond length varied from 90 to 120 degrees and from 0.95 to 1.15 Å respectively) and is also subject to a strong external field. In general, this normal mode procedure would lead to different sets of modes for different molecules with no trivial correspondence between the sets. For these

reasons, we use an approximate scheme to factor out distinct vibrational modes in order to obtain equivalents of the symmetric and asymmetric stretching and bending motions of an undistorted water molecule. The scheme was motivated by the normal mode analysis of a non-linear ABA molecule carried out in reference [61].

The three dimensional vibrational subspace can be written in terms of projector operators as $P_{vib} = I - P_{tr} - P_{rot}$. Transforming the Cartesian coordinates of the water molecule to the frame where the moment of inertia tensor is diagonal and the molecule is in the x-z plane (Fig. 1) we split the projector on the vibrational subspace into the contributions from the three orthonormal modes $P_{vib} = IP_{vib} = (P_{as} + P_{ss} + P_b)P_{vib}$ roughly corresponding to the asymmetric stretch (P_{as}), symmetric stretch (P_{ss}) and bend (P_b)

$$
\begin{aligned}
P_{as} &= |X_O\rangle\langle X_O| + |X_H^a\rangle\langle X_H^a| \\
P_{ss} &= |c_+\rangle\langle c_+| + |d_+\rangle\langle d_+| \\
P_b &= |c_-\rangle\langle c_-| + |d_-\rangle\langle d_-|
\end{aligned}
\tag{1}
$$

where the auxiliary coordinates

$$
\begin{aligned}
|X_H^s\rangle &= (|X_{H_1}\rangle - |X_{H_2}\rangle)/\sqrt{2} \\
|X_H^a\rangle &= (|X_{H_1}\rangle + |X_{H_2}\rangle)/\sqrt{2} \\
|Z_H^s\rangle &= (|Z_{H_1}\rangle - |Z_{H_2}\rangle)/\sqrt{2} \\
|Z_H^a\rangle &= (|Z_{H_1}\rangle + |Z_{H_2}\rangle)/\sqrt{2}
\end{aligned}
$$

are the symmetrized and antisymmetrized Cartesian displacements of the hydrogens, and

$$
\begin{aligned}
|c_\pm\rangle &= (|Z_H^a\rangle \pm |X_H^s\rangle)/\sqrt{2} \\
|d_\pm\rangle &= (|Z_O\rangle \pm |Z_H^s\rangle)/\sqrt{2}
\end{aligned}
$$

Here, X_i and Z_i, $i = O, H_1, H_2$ denote the Cartesian displacements of the i-th atom along the x and z-axes (Fig. 1). The asymmetric stretch projector picks out all "antisymmetric" movements along the x-axis. The sum of the symmetrized displacements $|Z_H^a\rangle + |X_H^s\rangle$ forms

6

the base of the symmetric stretch, while their difference $|Z_H^a\rangle - |X_H^s\rangle$ contributes to the bend. Figure 1 shows the vibrations defined above. The projectors (Eq. 1) have the necessary properties to make the vibrational modes defined by these projectors form an orthonormal basis, namely, $P_i^2 = P_i$, $P_iP_j = 0$, and $\sum_i P_i = I$.

In addition to separating the solvent motion into modes we also consider spatial localization. To do this, it is convenient to consider first, the solvent distribution around the electron center of mass. Because the transition rate from the first excited to the ground state is small for the hydrated electron, electronic transitions can occur relatively early as well as late in the trajectory. Late transitions originate from a nearly equilibrated excited state, while early ones do not correspond to any equilibrium configuration of the solvent, but do have a memory of the equilibrated ground state. Thus, the radial electron – oxygen pair distribution function calculated for the solvent configurations immediately preceding the electronic transitions (Fig. 2) is a mixture of the distribution functions of the equilibrated excited and ground states (which are reproduced in Fig. 2 from Fig. 7 of Ref. [48]) with the prevailing contribution coming from the former. Here and further in the paper, unless explicitly stated otherwise, the data represent an ensemble average over twenty non-adiabatic transitions. The distribution function facilitates the definition of solvation shells. Based on Fig. 2, the radius of the first solvation shell is taken to be 4.0 Å. The shell contains 6.2 water molecules on average. The second solvation shell, cut-off at 7.5 Å, includes 50.3 molecules on average. It is worth mentioning that the equilibrated excited state electronic wave function has the characteristic shape of a p-orbital.[48] Thus, in most of the generated trajectories, transitions occurred out of a roughly cylindrical rather than spherically symmetrical state. Unfortunately, we were unable to profoundly exploit this fact in our discussion, because a cylindrical pair distribution is a two dimensional distribution that requires many more data points to achieve statistics comparable with that of the one dimensional radial distribution. In section 3.1, we do present a qualitative picture reflecting contributions of different regions of the electron – oxygen cylindrical distribution to the transition rate.

2.2 Instantaneous non-adiabatic transition rate

We define an instantaneous transition rate constant using the Golden Rule expression (see e.g. Ref. [9])

$$k = \frac{2\pi}{\hbar} \frac{|V|^2}{\Delta E} \tag{2}$$

where ΔE is the electronic energy gap. To define the coupling matrix element V we expand the total Hamiltonian in time for the current instantaneous geometric configuration of solvent molecules and identify the coupling with the first order terms:

$$H(t_0 + \Delta t) = H(t_0) + \frac{\partial H}{\partial t} \Delta t + O[(\Delta t)^2]$$

$$V = \langle \beta | \frac{\partial H}{\partial t} \Delta t | \alpha \rangle = \langle \beta | \sum_Q \nabla_Q H \dot{Q} \Delta t | \alpha \rangle = \sum_Q \langle \beta | \nabla_Q H | \alpha \rangle \dot{Q} \Delta t = \sum_Q V_Q \tag{3}$$

where $\Delta t = 1$ fs is the time step of the algorithm and the summation goes over the solvent degrees of freedom Q defined by Eqs. (1). $|\alpha\rangle$ and $|\beta\rangle$ are the adiabatic wave functions for the initial and the final electronic states at the beginning of the step: $\langle \beta | H(t_0) | \alpha \rangle = 0$. The velocities $\dot{Q}$ used in Eq. (3) are those at the beginning of the step. Each V_Q reflects the contribution of a translational, rotational, or vibrational mode Q to the promotion of the non-adiabatic electronic transition.

The instantaneous rate constant k determines how fast the initial state starts to decay into the final state and is directly related to the transition probability:

$$P_{\beta\alpha}(\Delta t) = |\langle \beta | \partial/\partial t | \alpha \rangle \Delta t|^2 = |\langle \beta | \nabla_Q | \alpha \rangle \dot{Q} \Delta t|^2$$

$$= |\frac{\langle \beta | \nabla_Q H | \alpha \rangle}{\Delta E} \dot{Q} \Delta t|^2 = |V/\Delta E|^2 = (\hbar/2\pi\Delta E)k \tag{4}$$

Here, the first equality expresses the probability of changing states over the short time interval Δt. The second one is the result of chain differentiation applied to the time derivative of the adiabatic wave function that depends on time implicitly via the dependence on nuclear coordinates Q. The third equality follows from the Hellmann-Feynman theorem (see e.g. Ref. [62]). The last two are the corollaries of Eqs (3) and (2).

The non-adiabatic coupling element of Eq. (3) is in general a complex number $V = |V|e^{i\theta}$, however, it is the magnitude of the total V that determines the instantaneous transition rate (Eq. 2). Nevertheless, the magnitudes of the individual terms V_Q in the sum (3) do not correctly reflect the contributions from various shells and modes to the total coupling due to the complex phases. For the present analysis, we eliminated the complex part of the total coupling matrix element V by an appropriate rotation in the complex plane, thus making it real. We use the real parts of the individual terms in the sum (3) to analyze the roles of different shells and modes; that is,

$$|V| \;=\; Ve^{i\theta} = \sum_Q V_Q e^{i\theta} = \sum_Q Re\{V_Q e^{i\theta}\} \tag{5}$$

2.3 The work done on water molecules by the electron during a non-adiabatic transition

When the electron changes its state, hopping from the first excited state to the ground state, it releases energy which has to be accommodated by the solvent. An average energy gap between the states at the time of the transition is about 0.55 eV.[48] Because the force is determined self-consistently with the evolution of the electronic wave function, the electronic energy change ΔE is equal to the work done by this force to accelerate water molecules

$$\Delta E \;=\; \sum_Q F_Q \, \dot{Q} \, \Delta t \tag{6}$$

with the force given by[54]

$$F_Q \;=\; -Re\{\langle\beta U^+(t,t_1)|\nabla_Q H|U(t,t_0)\alpha\rangle/\langle\beta|U(t_1,t_0)|\alpha\rangle\} \tag{7}$$

where t_0 and t_1 indicate the beginning and the end of a time step and U is the time development operator.

Another route to analysis of the energy released is to take the molecular dynamics step twice – once allowing for the non-adiabatic transition with coordinates Q_{na} and the second

9

time restricting the dynamics to the original adiabatic electronic state with coordinates Q_a. The difference in the kinetic energies of solvent molecules for the non-adiabatic (K_{na}) and adiabatic (K_a) steps is approximately equal to the work done by the electron during the non-adiabatic transition,

$$\Delta E \quad \approx \quad K_{na} - K_a = \sum_Q \left(\frac{M_Q \dot{Q}_{na}^2}{2} - \frac{M_Q \dot{Q}_a^2}{2} \right) \tag{8}$$

Each term on the right hand side of Eq. (6) or Eq. (8) gives the amount of energy accepted by the particular solvent mode.

The time evolution of the energy released by the electron in the transition and during the subsequent adiabatic relaxation of the electronic ground state can be monitored by computing the kinetic energy stored in solvent modes along the non-adiabatic trajectory after the transition. This information will expose the behavior of different modes during equilibration of the solvent.

The equations for the coupling matrix element (Eq. 3) and the electronic energy change (Eqs. 6 and 7) have a very similar structure. In fact, in the limit of $\Delta t \rightarrow 0$, when the Pechukas force (Eq. 7) reduces to the impulsive force pointing along the Hamiltonian gradient[63], these two expressions become proportional to each other. Correspondingly, the instantaneous hop approximation often employed in surface hopping methods [40−42,56,63] cannot reveal any differences in the relative roles of nuclear degrees of freedom in promotion of the non-adiabatic transition and acceptance of the energy released. However, the use of the force, which is self-consistently determined during the finite duration transition, makes the analysis accessible. Even so, the similarity of promoting and accepting actions of solvent modes is inherent in the semiclassical approximation. Gas phase theories of radiationless transitions, especially those describing the "large molecule" limit, often restrict the summation to one or a few promoting modes and regard the rest as accepting modes, neglecting the extent to which promoting modes can also accept energy.[8−11] It will be shown that a promotion picture which involves at most a few physically interesting degrees of freedom

does not hold for the hydrated electron.

3 Results and discussion

3.1 Promotion of the non-adiabatic transition

Table 1 shows the decomposition of the coupling matrix element calculated at the time of the non-adiabatic transition and averaged over twenty such transitions.[48] To calculate the coupling due to a specific shell or mode we simply restrict the summation in Eq. (5) to the molecules or degrees of freedom which belong to that shell or mode. The largest contributions to the total non-adiabatic coupling matrix element come, in decreasing order, from the asymmetric stretch, rotation around the Z axis (see Fig. 1) and bending of water molecules. The contribution of the six first shell molecules is about 35 percent, while the second solvation shell containing about fifty molecules accounts for 60 percent leaving only 5 percent for the rest of the solvent. It is interesting to note that the contributions from the different modes of the first shell molecules are more evenly distributed than those of the second shell molecules. For example, we see that the coupling due to the bending vibration is comparable to the coupling due to the asymmetric stretch for the first shell molecules, while the asymmetric stretch of the second shell molecules is about ten times more important than the other two vibrations. Once a molecule gets close to the electron it does not matter very much what kind of motion the molecule undergoes. It efficiently couples the electronic states. Vibrations in general are more important than rotations, while translations can be safely neglected in the calculation of the total coupling.

In order to understand the difference in the relative contributions of various modes, one needs to consider the solvation structure together with the properties of the electronic wave function. The spatial characteristics of the electron density and the surrounding solvent have been studied in Ref. [48]. In that study it was found that the excited state of the hydrated electron is p-like in shape, while the ground state is approximately described by the s-like wave function. The p to s-state transition dipole moment defines the orientation

of the C_∞ symmetry axis of the p-state. Ichiye and coworkers[64] studied in detail the origin of interaction between water and simple negatively charged solutes. They found that for the first solvation shell about eighty percent of the interaction energy is of the ion - water molecule dipole character. This type of interaction dominates for the rest of the solvent, the higher order contributions being entirely negligible. According to this result the second shell water molecules and to a large extent the first shell ones point their dipole moments towards the hydrated electron. The excited state of the electron forms an elongated cavity, so that water molecules situated at the cavity's longer side are able to interact with a larger fraction of the electron density and, therefore, one expects, contribute most to the coupling matrix element (see Fig. 5 discussed later in this section).

Turning to the coupling matrix element of interest it can be expressed in a number of alternative ways. For the present purposes we focus on that in which the operator is the gradient of the Hamiltonian with respect to the solvent coordinate. Further, we focus on the electrostatic coupling of the electron and solvent, which should dominate other terms. For the idealized state symmetries (s and p) here, it follows that only contributions to the gradient of the electrostatic potential that are antisymmetrical with respect to the p orbital nodal place will yield non-vanishing contributions. For a water molecule in its equilibrium geometry, one finds that based only on symmetry (see Fig. 1) the derivative of the dipole moment with respect to displacement is parallel to the dipole moment for the bend and symmetric stretch coordinate, while it is perpendicular for the asymmetric stretch. For the present model, the magnitudes of the derivatives are similar.

Given these facts about solvent-ion interaction and solvent and electronic organization, along with the dipole derivatives, it follows that the asymmetric stretching motion of the laterally located molecules produce an electric dipole moment parallel to the p-orbital axis and, thus, strongly couples the electronic states. On the other hand, the other two vibrations vary molecular dipole in this direction only for the molecules located at the ends of the lobes of the electronic wave function. For this reason, the role of the symmetric stretch and bend

12

is less pronounced. Bend is slightly more important that the symmetric stretch, since the molecular dipole derivative with respect to the bending normal mode is somewhat larger. These trends are more clear for the second shell, where dipolar solvent orientation is more dominant.[64] The same argument applied to rotations correctly predicts the small influence of the rotation around the X-axis (for the definition of the coordinate system see Fig. 1), since this motion does not change the direction of the molecular dipole. The greater role of the Z-axis rotation compared to the Y-axis can be understood by comparing the corresponding moments of inertia. Their ratio is 1:3. The libration around the Z-axis proceeds with a greater value of the instantaneous velocity entering the expression for the coupling matrix element (Eq. 3).

Table 2 gives average absolute magnitudes of coupling per nuclear degree of freedom of the first and second shell molecules given by (cf. Eqs. 3 and 5)

$$V_N^{abs} \quad = \quad \frac{1}{N} \sum_{Q=1}^{N} |\langle\beta|\nabla_Q H|\alpha\rangle \dot{Q} \Delta t| \tag{9}$$

where N is the number of degrees of freedom within the corresponding shell and/or mode. The absolute magnitude of coupling per degree of freedom shows how strongly a single first or second shell degree of freedom would couple adiabatic electronic states if there were no other modes. According to these results, the first shell modes are about two and a half times more effective than the corresponding degrees of freedom of the second shell.

The instantaneous transition rates calculated via Eqs. (2) and (3) are given in Table 3. Although, as expected from Eq. (2), the data remains qualitatively similar to the data of Tables 1 and 2, the quantitative difference is striking. The asymmetric stretch alone reproduces half of the transition rate, standing dramatically out from all other motions, which seem far less important. This "discrepancy" is explained by the presence of the sign to the coupling matrix elements. The coupling matrix elements of Table 1 were obtained by averaging over twenty transitions, and in some cases the contributions to the averages had alternating signs. To calculate the data of Table 3, we averaged over the transition

13

rates proportional to the squares of the couplings according to Eq. (2). The asymmetric stretch always effectively coupled the electronic states, but in one fifth of all the transitions it contributed to the total coupling matrix element of Eq. (5) destructively. Destructive contributions due to, for instance, the rotation around the Z axis were also observed, although four times less frequently then for the asymmetric stretch.

The constructive and destructive contributions to the total coupling is brought about by the distinctly multi-mode origin of promotion of the electronic transition. Numerous quantum mechanical treatments of gas phase vibronic relaxation consider a single mode approximation for induced mixing for systems of many degrees of freedom (see Ref. [8, 9, 10, 11] and references therein). This is clearly not valid for the case of the hydrated electron. Tables (1)-(3) show that the transition is not localized in any respect. In a single mode promotion, there is one nuclear degree of freedom responsible for the mixing of electronic states, and the coupling matrix element reduces to a product of two scalars — the nuclear velocity and the corresponding derivative of the electronic Hamiltonian. The greater the gradient and the velocity, the faster the transition. Multi-mode systems can exhibit a nonintuitive behavior: the coupling can entirely vanish even if the electronic Hamiltonian gradients and nuclear velocities are large. The coupling vanishes when nuclear and electronic dynamics are uncorrelated, that is, when nuclear velocities are distributed at random with respect to the directions of the corresponding gradients of the electronic Hamiltonian. This follows from the fact that the coupling matrix element of Eq. (3) can be regarded as a scalar product of two vectors defined in the configuration space of nuclear degrees of freedom

$$V = \langle \nabla H | \dot{R} \rangle \Delta t; \quad \langle \nabla H | = \sum_Q \langle \beta | \nabla_Q H | \alpha \rangle \langle \hat{Q} |, \quad | \dot{R} \rangle = \sum_Q \dot{Q} \, | \hat{Q} \rangle \qquad (10)$$

where $\hat{Q}$ is the unit vector along the Qth nuclear coordinate. Thus, it is evident that the angle between the gradient of the electronic Hamiltonian $|\nabla H\rangle$ and the nuclear velocity $|\dot{R}\rangle$ vectors has a crucial influence on the magnitude of the coupling. Table 4 gives the deviation of the angle from 90° for different nuclear modes and solvation shells. The angles reported are obtained as $\cos^{-1}\{\overline{V}/\overline{\dot{R}}\ \overline{\nabla H}\}$ with bars above the letters indicating averaging

over twenty transitions. The significance is large; if the first solvation shell performed a collective motion acting as a single mode its contribution to the transition rate would be fifty times greater ($\cos[90.0 - 1.4] \approx 1/50$). This effect is an order of magnitude stronger for the second shell. Among the various modes, the asymmetric stretch is most correlated with the electron dynamics explaining why it accounts for a large fraction of the instantaneous transition rate (Table 3).

The correlation between nuclear velocities and the gradient of the electronic Hamiltonian appears due to the coupling between the electronic and nuclear dynamics, which is mainly determined by the force (Eq. 7) exerted by the electron on solvent molecules. Table 5 presents average magnitudes of the force per nuclear degree of freedom for various shells and modes at the transition step, defined by

$$F_N^{abs} = \frac{1}{N} \sum_{Q=1}^{N} |F_Q| \tag{11}$$

where F_Q is given by Eq. (7) and N is the number of modes in a particular average. There is an obvious correlation between the data of Tables 4 and 5 supporting our previous statement.

Fig. 3 shows the radial electron – oxygen pair coupling distribution $v(R)$ together with the pair distribution of coupling magnitude $v^{abs}(R)$, where R is the scalar distance between the oxygen nucleus and the electronic center of mass. The integral of $v(R)$ weighed by the radial pair distribution function $g(R)$ (Fig. 2) gives the magnitudes of the total coupling matrix element $|V|$ of Eq. (5):

$$\begin{aligned} |V| &= \int_0^\infty dR \; 4\pi R^2 \; g(R) \; v(R) \; \rho \\ \sum_Q |V_Q| &= \int_0^\infty dR \; 4\pi R^2 \; g(R) \; v(R)^{abs} \; \rho \end{aligned} \tag{12}$$

with ρ being the solvent density. The corresponding integral of $v^{abs}(R)$ results in the sum of absolute values of V_Q defined in Eq. (3). The absolute magnitude of the coupling is at a maximum in the first solvation shell and smoothly decays with the distance R. The coupling almost vanishes for the molecules which are situated on the border between the first and

the second solvation shells. This can be explained as follows. The molecules within the first and the second shell differ in their orientation toward the electron, and, hence, the border region exhibits a less ordered structure. Although a single molecule of the border region makes a significant contribution to the total coupling matrix element, on the average the net contribution becomes negligible due to the variations in molecular orientation.

The functions $v(R)$ and $v^{abs}(R)$ reflect the coupling due to a single water molecule at the distance R from the electron center of mass. While these functions decrease with R, the number of molecules increases. To visualize the role of all molecules located at the distance R from the electron we plot the distribution of the cumulative coupling (Fig. 4) defined as

$$
\begin{aligned}
v^{cum}(R) &= 4\pi R^2 \; v(R) \; g(R) \; \rho \\
|V| &= \int_0^\infty dR \; v^{cum}(R)
\end{aligned}
\tag{13}
$$

Although a single molecule of the first solvation shell couples the electronic states much more strongly than a single molecule of the second shell (Table 2, Fig. 3), the cumulative contribution of the second shell is twice that of the first shell (Table 1, Fig. 4). At large distances the radial electron – oxygen pair distribution of the coupling per molecule (Fig. 3) decays faster then $1/R^2$ so that the role of the molecules beyond the second solvation shell is insignificant.

Since the excited state electronic wavefunction is p-like in shape, it is more cylindrically than spherically symmetric. To better illustrate how different spatial regions of the solvent promote the electronic transition we display a contour plot of the cylindrical pair distribution function of coupling $v^{cyl}(R,|Z|)$ (Fig. 5). The Z-axis of the distribution is defined by the direction of the first excited to the ground state transition dipole moment and parallels the C_∞ approximate symmetry axis of the p-like excited state. Because the two dimensional cylindrical distribution has inherently poorer statistics than the one dimensional radial distribution, in Fig. 5 we coarse-grain the coordinate axes by 0.1Å and then compute running averages over sets of 20 adjacent points. We also average over the sign of the Z coordinate. The cylindrical distribution of coupling $v^{cyl}(R,|Z|)$ is defined in such a way, that its integral

weighed by the corresponding cylindrical electron – oxygen pair distribution $g^{cyl}(R, Z)$ gives the magnitude of the total coupling matrix element of Eq. (5):

$$|V| \;=\; \int_0^\infty 2\pi R \, dR \int_{-\infty}^\infty dZ \; g^{cyl}(R, Z) \; \frac{v^{cyl}(R, |Z|)}{2} \; \rho \qquad (14)$$

We recall that the electron density for p-state is elongated. The distribution of coupling evident in Fig. 5 is consistent with the expectation that solvent located centrally with respect to this elongated electron density is more strongly coupled than that near only to one end ($Z \sim \pm 5$Å). Further, it is reasonable to expect the effect of the changing solvent induced electric field is of particular importance due to the presence of an electronic nodal region.

Finishing our discussion of the promotion of the non-adiabatic electronic transition we present Figure 6, which shows the temporal evolution of the instantaneous rate (Eq. 2) of the downward transition over one hundred femtoseconds before the hop as well as the instantaneous rate of the reverse process for the forty femtoseconds after it. (Note the logarithmic scale of the y-axis.) The figure is based on the data from a single trajectory. We observe two time scales in the fluctuation of the transition rate with periods of about ten and fifty femtoseconds, which correspond to the vibrational and librational motions of the solvent. Vibrations cause fluctuations of much larger amplitude. During each vibrational period, the rate is high for two or three femtoseconds, when the time derivative of the vibrational coordinate $\dot{Q}$ is large (cf. Eq. 3). It is interesting that the probability to make the downward transition does not show any trends during the period prior to the transition point, with a fluctuation occurring at roughly 50 fs leading to a transition probability nearly as large as that acting at the observed transition point. However, once the transition occurs the probability for an upward transition rapidly decays; this decay of the instantaneous transition rate (Eq. 2) of the reverse process is due to the rapid separation of the electronic energy levels (ΔE) brought about by the fast inertial response of the solvent immediately following the transition.[48]

17

3.2 Energy transfer during and after the non-adiabatic transition

During the one femtosecond step of a non-adiabatic transition the electronic energy abruptly changes by about 0.5 eV. This excess energy is transferred to the solvent leading to local heating. Tables 6 and 7 show the energies accepted by different shells and modes calculated by the formulas (6) and (8) of section 2.3, respectively. Both tables show similar data, with the minor discrepancies being mainly due to the finite difference scheme used in the molecular dynamics algorithm to calculate solvent molecules velocities. About forty percent of the total energy disposed by the electron is transferred to the first solvation shell. The second shell accepts another fifty percent. As in the case with the promotion discussed in the previous subsection, energy release during the non-adiabatic transition of the hydrated electron is not localized but involves both the first and the second shells. Nevertheless, the relative impact of the electronic transition on the first shell molecules is substantial, leading to an initial local heating of 40 K. Over the next several femtoseconds the electron experiences a rapid adiabatic relaxation, continuing to release energy and the local heating reaches almost 100 K (see Fig. 9 discussed later in this section). We emphasize that this local heating does not have such dramatic consequences on reorientational and diffusive motions in the solvent as a uniform heating would have. The overall temperature rise is only several Kelvin and the relaxation dynamics proceeds on a usual time-scale.[34] For instance, it takes several hundred femtoseconds until the first and the second shells equilibrate. (See Ref. [34] for a discussion of the influence of local heating on solvation dynamics.) Within the first solvation shell, it is the asymmetric stretch which gets most agitated during the transition. Both the asymmetric stretch and the rotation around the Z axis (see Fig. 1) of an average solvent molecule each equally account for one third of the non-adiabatic electronic energy change. The rotation around the Z axis is most involved in part because it corresponds to the smallest moment of inertia. It is easily shown, that if two rotors hold equal amounts of energy $E_1 = E_2$ (equipartition ansatz) and if the torques acting on the rotors are the same

18

$\dot{M}_1 = \dot{M}_2$, the energy transfer is faster for the rotor with the smaller moment of inertia:

$$\frac{dE_1/dt}{dE_2/dt} = \frac{\frac{d}{dt}(M_1^2/2I_1)}{\frac{d}{dt}(M_2^2/2I_2)} = \frac{(M_1/I_1)\dot{M}_1}{(M_2/I_2)\dot{M}_2} = \sqrt{\frac{I_2}{I_1}}$$

Here I and M denote the moment of inertia and the angular momentum correspondingly.

The next two figures show the radial electron – oxygen pair distributions of energy accepted during the non-adiabatic transition by a single molecule ε (Fig. 7) and by all molecules ε^{cum} (Fig. 8) at the distance R from the electron. These distribution functions are defined analogously to the corresponding radial distributions of coupling (Eqs (12) and (13), where v, v^{cum} and V correspond to ε, ε^{cum} and the total accepted energy ΔE). In general, the closer a molecule is to the electron, the more energy it accepts. The decay of the distribution function in Fig. 7 with distance is sufficiently gradual, that the cumulative effect of molecules as far as 6 Å from the electron center of mass is still significant (Fig. 8). Comparing the radial distribution of energy accepted during the transition (Figs 7 and 8) with the distribution of coupling between the electronic states (Figs 3 and 4) we note that the former does not have the minimum around 4 Å (in the intershell region) which was quite noticeable in the latter. During the non-adiabatic transition the electron strongly acts on all surrounding water molecules independent of their location. The tenfold difference in the magnitudes of the coupling matrix element ($\simeq 0.05$ eV) and the transferred energy ($\simeq 0.5$ eV) explains this observation.

After the electron makes the transition to the ground state, it continues to release energy adiabatically due to solvation on the newly formed ground state. Calculations predict two time-scales for this equilibration process.[48] The first part of it is due to the inertial solvent response. It lasts for about 20 fs, during which the electron loses most of the 2 eV of the total lowering of the ground adiabatic state. The second longer part extends for about 250 fs. Temporal variation of the energy contained within the first and the second solvation shells is given in Figure 9, where we plot local temperature as a function of time after the transition. The first solvation shell undergoes a strong heating for 10 fs. The second shell becomes hotter to a significantly lesser extent. Further, its response is mostly secondary,

responding to the first shell cooling, transferring energy to the second shell and to the rest of the solvent. It is the delay in response of the second shell rather than the fast heating of the first one that matches the 20 fs inertial part of the relaxation. The first shell water molecules vigorously accelerate during the first 10 fs after the transition and continue to move very fast for another 10 fs adjusting themselves on the new adiabatic potential surface. More global changes in solvent structure, including second shell molecules, are responsible for the slower component of the hydrated electron ground state relaxation.

Various degrees of freedom within the first solvation shell do not respond equally to the adiabatic electronic state relaxation. For several dozen femtoseconds after the non-adiabatic transition, rotations hold a much larger fraction of the energy than vibrations and translations. Figure 10 demonstrates this. An understanding of this comes from the difference in the frequencies of vibrational and librational motions of bulk water. Water molecules complete their vibrational cycle within ten femtoseconds, during half of which molecule velocity vectors point in the direction opposite to the force due to the electron. Because the electron continues rapid adiabatic relaxation longer than half of the vibrational period, the accepted energy averaged over the period is small. On the contrary, the librational period is about fifty femtoseconds. Twenty femtosecond intensive energy discharge covers less than half of this. The force – velocity dot product does not oscillate and the contribution of librations to the total work of Eq. (6) is large. Thus, the librations are primarily responsible for effective energy transfer.

4   Conclusions

In summary, our theoretical study on the involvement of particular solvent degrees of freedom in non-radiative relaxation of the hydrated electron has shown that the electron relaxes due to a spatially delocalized multi-mode coupling between the adiabatic states. The largest contribution to the coupling comes from the asymmetric stretch of water molecules. Bending vibration and rotation around symmetry axis are also important degrees of freedom. The

transition rate is not determined by motions solely within the first solvation shell, the second shell contribution being twice as large. The temporal behavior of the transition probability exhibits two time scales corresponding to vibrational and librational bands of the bulk water spectrum.

The evolution of energy released during the transition proceeds in two steps. The first one takes about 10 fs and is characterized by a vigorous heating of the first solvation shell. The second one involves global reorganization of solvent structure and lasts several hundred femtoseconds. Energy transferred to the first shell is accepted primarily by solvent librations. The reason for this is a good match between the libration period and the duration of adiabatic electronic energy loss following the transition. Therefore, in short, vibrations stimulate the hydrated electron change of state, while first shell librations are responsible for immediate acceptance of released energy. However, in both cases, it is the proton motion that is dominant.

Studies of relaxation for more complex solutes will be of interest in determining the generality of these results, and the division between intramolecular and solvent modes.

Acknowledgments

References

[1] Cario, G.; Frank, J. *Z. Physik* **1923**, 17, 202.

[2] Kistiakowsky, G. B.; Parmenter, C. S. *J. Chem. Phys.* **1965**, 42, 2942.

[3] Douglas, A. E. *J. Chem. Phys.* **1967**, 45, 1007.

[4] Robinson, G. W.; Frosch, R. P. *J. Chem. Phys.*, **1963**, 38, 1187.

[5] Freed, K. F.; Gelbart, W. M. *Chem. Phys. Lett.* **1971**, 10, 187.

[6] Nitzan, A.; Jortner, J. *Chem. Phys. Lett.*, **1971**, 11, 458.

[7] Robinson, G. W. *Excited States*, **1974**, 1, 1.

[8] Freed, K. F. In *Radiationless Processes in Molecules and Condensed Phases*; Fong, F. K., Ed.; Springer-Verlag: Berlin, 1976.

[9] Avouris, P.; Gelbart, W. M.; El-Sayed, M. A. *Chem. Rev.*, **1977**, 77, 793.

[10] *Radiationless Transitions*; Lin, S. H., Ed.; Academic Press: New York, 1980.

[11] Fisher, G. *Vibronic Coupling*; Academic Press: New York, 1984.

[12] Bersuker, I. B.; Polinger, V. Z. *Vibronic Interactions in Molecules and Crystals*; Springer-Verlag: New York, 1986.

[13] Diestler, D. J. In *Radiationless Processes in Molecules and Condensed Phases*; Fong, F. K., Ed.; Springer-Verlag: Berlin, 1976.

[14] Ulstrup, J. *Charge Transfer Processes in Condensed Media*; Springer-Verlag: New York, 1979.

[15] Kasha, M. *Discuss. Faraday Soc.* **1950**, 9, 14.

[16] Robinson, G. W.; Frosch, R. P. *J. Chem. Phys.* **1962**, 37, 1962.

[17] Hunt, G. R.; McKoy, E. F.; Ross, I. G. *Aust. J. Chem.* **1962**, 15, 591.

[18] Sharp, K.; Honig, B. A. *Rev. Biophys. Chem.* **1990**, 19, 301.

[19] Prezhdo, V. V.; Tyurin, S. A.; Prezhdo, O. V.; Tarasova, G. V.; Akulova, O. N.; Kurskaya, T. N. *Acta Phys. Pol. A* **1994**, 85, 509.

[20] Prezhdo, V. V.; Tyurin, S. A.; Prezhdo, O. V.; Tarasova, G. V.; Akulova, O. N.; Kurskaya, T. N. *Acta Phys. Pol. A* **1994**, 86, 327.

[21] Buchner, M.; Ladanyi, B. M.; Stratt, R. M. *J. Chem. Phys.* **1992**, 97, 8522.

[22] Cho, M.; Fleming, G. R.; Saito, S.; Ohmine, I.; Stratt, R. M. *J. Chem. Phys.* **1994**, 100, 6672.

[23] Zurek, W. H. *Physics Today* **1991**, October, 36.

[24] Bittner, E. R.; Rossky, P. J. *J. Chem. Phys.* **1995**, 103, 8130.

[25] Leggett, A. J.; Chakravarty, S.; Dorsey, A. T.; Fisher, M. P. A.; Garg, A.; Zwerger, W. *Rev. Mod. Phys.* **1987**, 59, 1.

[26] Makarov, D. E.; Makri, N. *Phys. Rev. A* **1993**, 48, 3626.

[27] Hu, B. L.; Paz, J. P.; Zhang, Y. *Phys. Rev. D* **1992**, 45, 2843.

[28] Migus, A.; Gauduel, Y.; Martin, J. L.; Antonetti, A. *Phys. Rev. Lett.* **1987**, 58, 1559.

[29] Pommeret, S.; Antonetti, A.; Gaudel, Y. *J. Am. Chem. Soc.* **1991**, 113, 9105.

[30] Long, F. H.; Lu, H.; Eisenthal, K. B. *Phys. Rev. Lett.* **1990**, 64, 1469.

[31] Long, F. H.; Lu, H.; Shi, X.; Eisenthal, K. B. *Chem. Phys. Lett.* **1991**, 185, 47.

[32] Alfano, J. C.; Walhout, P. K.; Kimura, Y.; Barbara, P. F. *J. Chem. Phys.* **1993**, 98, 5996.

[33] Kimura, Y.; Alfano, J. C.; Walhout, P. K.; Barbara, P. F. *J. Phys. Chem.* **1994**, 98, 3450.

[34] Maroncelli, M.; Fleming, G. R. *J. Chem. Phys.* **1988**, 89, 5044.

[35] Motakabbir, K. A.; Schnitker, J.; Rossky, P. J. *J. Chem. Phys.* **1989**, 90, 6916.

[36] Webster, F. A.; Schnitker, J.; Friedrichs, M. S.; Friesner, R. A.; Rossky, P. J. *Phys. Rev. Lett.* **1991**, 66, 3172.

[37] Webster, F. A.; Rossky, P. J.; Friesner, R. A. *Comp. Phys. Comm* **1991**, 63, 494.

[38] Neria, E.; Nitzan, A.; Barnett, R. N.; Landman, U. *Phys. Rev. Lett.* **1991**, 67, 1011.

[39] Neria, E.; Nitzan, A. *J. Chem. Phys.* **1993**, 99, 1109.

[40] Tully, J. C. *J. Chem. Phys.* **1990**, 93, 1061.

[41] Space, B.; Coker, D. F. *J. Chem. Phys.* **1991**, 94, 1976.

[42] Coker, D. F. In *Computer Simulations in Chemical Physics*; Allen, M. P.; Tildesley, D. J., Eds.; Kluwer Academic Publishers: Netherlands, 1993.

[43] Maroncelli, M.; MacInnis, J.; Fleming, G. R. *Science* **1989**, 243, 1674.

[44] Barbara, P. F.; Walker, G. C.; Smith, T. P. *Science* **1992**, 256, 974.

[45] Rossky, P.J.; Simon, J. D. *Nature* **1994**, 370, 263.

[46] Keszei, E.; Nagi, S.; Murphrey, T. H.; Rossky, P. J. *J. Chem. Phys.* **1993**, 99, 2004.

[47] Keszei, E.; Murphrey, T. H.; Rossky, P. J. *J. Phys. Chem.* **1995**, 99, 22.

[48] Schwartz, B. J.; Rossky, P. J. *J. Chem. Phys.* **1994**, 101, 6902.

[49] Schwartz, B. J.; Rossky, P. J. *J. Chem. Phys.* **1994**, 101, 6917.

[50] Schwartz, B. J.; Rossky, P. J. *J. Phys. Chem.* **1994**, 98, 4489.

[51] Schwartz, B. J.; Rossky, P. J. *Phys. Rev. Lett.* **1994**, 72, 3282.

[52] Schwartz, B. J.; Rossky, P. J. *J. Phys. Chem.* **1995**, 99, 2953.

[53] Schwartz, B. J.; Bittner, E. R.; Prezhdo, O. V.; Rossky, P. J. *J. Chem. Phys.* **1996**, in press.

[54] Pechukas, P. *Phys. Rev.* **1969**, 181, 174.

[55] Feynman, R. P.; Hibbs, A. R. *Quantum Mechanics and Path Integrals*; McGra-Hill, Inc.: New York, 1965.

[56] Tully, J. C.; Preston, R. K. *J. Chem. Phys.* **1971**, 55, 562.

[57] Tully, J. C. In *Dymanics of Molecular Collisions*; Miller, W. H., Ed.; Plenum: New York, 1976.

[58] Murphrey, T. H.; Rossky, P. J. *J. Chem. Phys.* **1993**, 99, 515.

[59] Toukan, K.; Rahman, A. *Phys. Rev. B* **1985**, 31, 2643.

[60] Schnitker, J.; Rossky, R. J. *J. Chem. Phys.* **1987**, 86, 3462.

[61] Landau, L. D.; Lifshitz, E. M. *Course in Theoretical Physics. Mechanics*; Pergamon Press: New York, 1988.

[62] Epstein, S. P. In *The Force Concept in Chemistry*; Deb, B. M.,Ed.; Van Nostrand Reinhold: New York, 1981.

[63] Coker, D. F.; Xiao, L. *J. Chem. Phys.* **1995**, 102, 496.

[64] Hyun, J.-K.; Babu, C. S.; Ichiye, T. *J. Phys. Chem.* **1995**, 99, 5187.

Table 1: Components of coupling matrix element (meV) between the first excited and ground states (Eqs. 3 and 5).

due to	trans	rot[x]	rot[y]	rot[z]	v [a]	v [s]	v [bd]	all modes
1st shell	0	1	3	4	6	1	4	19
2nd shell	0	1	2	13	14	0	2	32
all molecules	0	3	6	14	20	2	9	54

Table 2: Average absolute magnitudes of coupling (meV) per nuclear degree of freedom (Eq. 9) between the first excited and ground states.

due to	trans	rot[x]	rot[y]	rot[z]	v [a]	v [s]	v [bd]	all modes
1st shell	0.1	0.7	2.2	3.5	3.3	1.7	1.1	1.4
2nd shell	0.1	0.3	0.7	1.5	1.4	0.6	0.4	0.6

Table 3: Instantaneous rates (ps^{-1}) of the first excited to ground state transition at the step of the non-adiabatic transition calculated from Eqs. (2), (3) and averaged over 20 transitions.

due to	trans	rot[x]	rot[y]	rot[z]	v [a]	v [s]	v [bd]	all modes
1st shell	0.00	0.00	0.01	0.00	0.02	0.01	0.01	1.77
2nd shell	0.00	0.00	0.07	0.02	0.56	0.05	0.05	5.93
all molecules	0.00	0.08	0.08	0.22	5.94	0.08	0.74	12.08

Table 4: Average deviations of the angle (in degrees) between ∇H and $\dot{Q}$ of Eq. (10) from the right angle. The larger the deviation the more the nuclear dynamics is correlated with the dynamics of the electronic structure.

	trans	rot[x]	rot[y]	rot[z]	v [a]	v [s]	v [bd]	all modes
1st shell	12.8	5.8	7.8	10.8	17.9	12.0	15.9	1.4
2nd shell	1.4	0.5	1.8	2.3	8.7	2.1	3.0	0.2

Table 5: Absolute magnitudes of the quantum (Eq. 7) force (eV/Å) per nuclear degree of freedom, as defined by Eq. (11).

	trans	rot[x]	rot[y]	rot[z]	v [a]	v [s]	v [bd]	all modes
1st shell	0.12	0.06	0.25	0.22	0.41	0.12	0.13	0.15
2nd shell	0.03	0.02	0.07	0.08	0.12	0.03	0.03	0.05

Table 6: Work (in meV) due to the quantum force (Eq. 7) done by the electron on the solvent during the one femtosecond non-adiabatic transition calculated via Eq. (6).

work done on (T change)	trans	rot[x]	rot[y]	rot[z]	v [a]	v [s]	v [bd]	all modes
1st shell	2	9	22	32	76	17	28	177
2nd shell	2	6	23	98	78	17	28	252
all molecules	4	17	57	146	158	38	65	485

Table 7: Difference in kinetic energies (in meV) resulting from the one femtosecond non-adiabatic transition calculated via Eq. (8). Local heating (in K) of the solvent is given in parentheses.

work done on (T change)	trans	rot[x]	rot[y]	rot[z]	v [a]	v [s]	v [bd]	all modes
1st shell	3	13	28	42	76	10	29	200
	(2)	(24)	(53)	(75)	(141)	(18)	(62)	(42)
2nd shell	4	5	27	107	78	7	32	261
	(0)	(1)	(6)	(25)	(18)	(2)	(8)	(7)
all molecules	7	19	73	173	171	19	64	525
	(0)	(1)	(4)	(10)	(10)	(1)	(4)	(3)

Figure 1: Vibrational modes of a distorted water molecule defined by Eqs. (1).

Figure 2: Electron – oxygen radial distribution function for configurations immediately before the electronic transition together with the corresponding distributions for the equilibrated excited and ground states of the hydrated electron.

Figure 3: Radial electron – oxygen pair distribution of coupling per molecule $v(R)$ (solid line) and radial distribution of coupling magnitude $v_{abs}(R)$ (dashed line) of Eqs. (12).

Figure 4: Radial electron – oxygen pair distribution of the cumulative coupling (v^{cum}) from Eq. (13). The integral of v^{cum} is given by the dashed line.

Figure 5: Contour plot of the cylindrical electron – oxygen pair distribution function of coupling between the P-like excited and ground states of the hydrated electron $v^{cyl}(R, |Z|)$ from Eq. (14). Darker regions correspond to stronger coupling. The Z-axis of the plot corresponds to an approximate C_∞ symmetry axis of the "dumb-bell" shaped excited state electron density.[48]
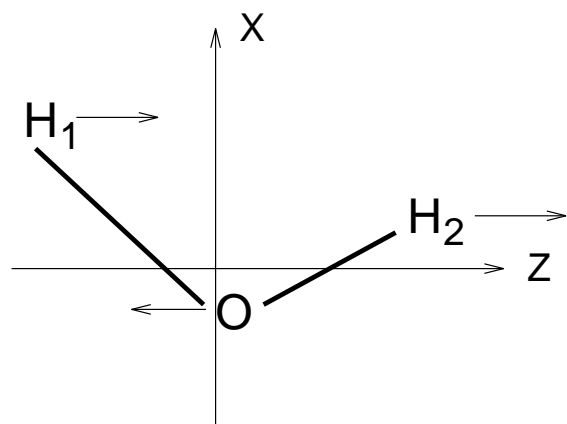
Figure 6: Instantaneous rate (Eq. 2) of the downward (negative time) and upward (positive time) transitions for a single representative trajectory.

Figure 7: Radial electron – oxygen pair distribution of energy accepted during the electronic transition by a *single* molecule at the distance R from the electron.
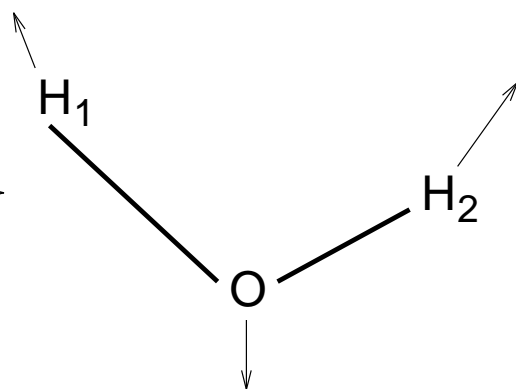
Figure 8: Radial electron – oxygen pair distribution (ε^{cum}) of energy accepted during the electronic transition by *all* molecules at the distance R from the electron (solid line). The integral of ε^{cum} is given by the dashed line.

Figure 9: Energy evolution within the solvent after the non-adiabatic electronic transition. Solid line indicates temperature of the whole solvent, dashed line gives temperature of the first solvation shell, and dotted line gives temperature of the second shell.
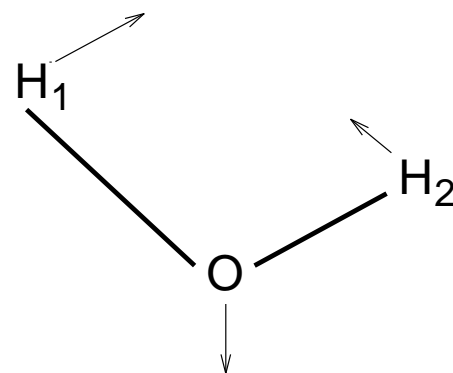
Figure 10: Energy distribution within the first solvation shell as a function of time since the non-adiabatic transition. Solid line gives translational temperature, dashed line indicates vibrational temperature, and dotted line gives rotational temperature.

asym stretch   sym stretch   bend

integral of $\varepsilon^{cum}(R)$

$\varepsilon^{cum}(R)$ / meV

R / Å